Acoustic spectral imaging and transfer learning for reliable bearing fault diagnosis under variable speed conditions.

HASAN, M.J., ISLAM, M.M.M. and KIM, J.-M.

2019

Acoustic Spectral Imaging and Transfer Learning for Reliable Bearing Fault Diagnosis under Variable Speed Conditions

Md Junayed Hasan[1*], M M Manjurul Islam[2*], and Jong-Myon Kim[3*]

Affiliation:

*School of Electrical, Electronics and Computer Engineering, University of Ulsan, Ulsan (44610), South Korea

Address:

*Building No. 7, 93 Daehak-ro, Nam-gu, Ulsan (44610), South Korea

Email:

[1]junhasan@gmail.com

[2]m.m.manjurul@gmail.com

[3]jmkim07@ulsan.ac.kr

Corresponding Author:

Jong-Myon Kim, School of Electrical, Electronics and Computer Engineering, University of Ulsan, Ulsan (44610), South Korea.

Email: jmkim07@ulsan.ac.kr

Tel: +82-52-259-2217

Fax: +82-52-259-1687

Abstract

Incipient fault diagnosis of a bearing requires robust feature representation for an accurate condition-based monitoring system. Existing fault diagnosis schemes are mostly confined to manual features and traditional machine learning approaches such as artificial neural networks (ANN) and support vector machines (SVM). These handcrafted features require substantial human expertise and domain knowledge. Further, these feature characteristics vary with the bearing's rotational speed. Hence, such methods do not yield the best results under variable speed conditions. Therefore, this paper presents a reliable fault diagnosis scheme based on acoustic spectral imaging (ASI) of acoustic emission (AE) signals as a precise health state. These health states were further utilized with transfer learning, which is a machine learning technique, which shares knowledge with deep convolutional neural networks (DCNN) for accurate diagnosis under variable operating conditions. In ASI, the amplitude of the spectral components of the windowed time-domain acoustic emission signal are transformed into spectrum imaging. ASI provides a visual representation of acoustic emission spectral features in images. This ensures enhanced spectral images for transfer learning (TL) testing and training, and thus provides a robust classifier technique with high diagnostic accuracy.

Keywords:

1. Introduction

Electromechanical motors such as induction motors have widespread applications in wind turbines, pumps, and generators where they are accountable for almost 70% of the gross energy consumption[1, 2]. Bearings are used to minimize friction in motors which undergo rotation. Moderation of friction preserves energy along with supporting a propitious machine lifetime. However, bearings may exhibit surface spall or cracks due to coarse operating environments and cyclic stuffing [3]. Bearings are the most frequent failed components in rotating machines and account for more than 50% of failures[1, 4]. If these faults in bearings are not detected in the early stage, they can lead to unexpected shutdowns, which are unfavorable in terms of cost and production[5-8].

Bearing fault diagnosis is performed by collecting data (i.e., vibration acceleration signals, acoustic emission signals, and motor currents), which has been an important aspect of studies conducted over the last few decades[7, 9-11]. These fault diagnosis studies prove that diagnosis of the bearing can reduce maintenance expenses by enhancing the reliability of machinery[7, 10, 12-15]. In the field of bearing fault diagnosis, vibration signals[1, 7, 16] and motor current analysis[17, 18] have been widely exploited. Multiple signature analyses of vibrations and motor currents have also been considered in research to guarantee the highest reliability[19]. These analyses mainly established high reliability in fault diagnosis for high-speed bearings. For low-speed bearings, capturing intrinsic information from vibration signals and the motor current is difficult. Acoustic emission (AE) signals can capture intrinsic information from low-energy signals[20-24], which makes AE signals more significant for data-driven diagnosis approaches. This study employs an AE-based fault diagnosis approach for low-speed bearings.

Fault diagnosis of low-speed bearings under variable speed conditions (e.g., revolutions per minutes (RPM)) is still a challenge. Traditional data-driven fault diagnosis approaches have main processes, for example, handcraft feature extraction by a signal processing technique and identification of fault types using extracted features. Acoustic signal-based diagnosis methods mostly consider an envelope analysis-based approach by analyzing the peaks at the character frequencies associated with each defect type in the power spectrum of the envelope signal[25-27]. Because of the relationship with the defect frequency and rotational speed of the bearing[25-27], these approaches are inefficient under variable rotational speeds. Similarly, conventional feature extraction-based methods cannot resolve the earlier mentioned issues as well, which results in ineffective diagnosis performances for variable speed conditions. Moreover, it is necessary to have proper domain expertise to select pertinent features[28-30].

This study presents a new approach for the diagnosis of low-speed bearings. Two major limitations of existing approaches are addressed in this work: a) the requirement of domain level expertise for feature extraction and selection under different operational speeds and b) the requirement of special dynamic algorithms for automation of the feature extraction process. Two-dimensional (2D) acoustic spectral images (ASI) were used instead of one-dimensional (1D) signals in this work. The 2D ASI employed to observe the pattern for different health states to make the feature selection process easier for speed invariance conditions. The proposed 2D ASI creates identical patterns for the same type of health, where variable operating speeds

do not affect identical patterns for certain types of the health state. Feature selection process automation is performed by applying a transfer learning (TL)-based Convolutional Neural Network (CNN) based on these 2D spectral images. Although the CNN makes the feature extraction and selection process easier due to its convoluted encoding layers, it is difficult to deal with a large amount of data[31, 32]. However, since these straightforward neural networks struggle to deal with massive amounts of data, to make the learning faster and effective, a transfer learning-based neural network is proposed here. We propose a transfer learning-based neural network that was first introduced by Zheng et al.[33] to deal with similar issues to make the learning faster and effective for 1D raw signal. However, with the raw AE signal of low-speed bearings, this approach cannot uncover the critical features of transferring the knowledge domain for further classification. In this study, after creating the invariance scenario with 2D ASI, a TL-based approach was carried out to resolve these challenges. The details of the TL and proposed CNN architecture are discussed in the methodology section.

The main contributions of this work can be summarized as follows.

1) A novel identical 2D acoustic spectral imaging (ASI)-based pattern formation method for different health types is developed to explore the potential information of AE signals.

2) This 2D ASI is further utilized with a deep convolution neural network (DCNN) to automate the feature extraction and selection process.

3) DCNN-aided transfer learning (TL) is proposed for fault diagnosis for low-speed bearings with variations of the shaft speed (e.g., RPMs). The proposed method, including ASI for the RPM independent pattern and DCNN-aided TL for fault diagnosis under variable RPMs, was suitably validated with extensive experiments and simulations, which justifies the potential of the proposed methodology over existing approaches in terms of achieving satisfactory theoretical results compared to experiments.

The remaining part of the paper is organized as follows. Section 2 provides details of the methodology, including the AE data acquisition system, acoustic spectral (ASI)-based bearing health state visualization, and transfer learning (TL)-based bearing classification. The experimental results are provided in Section 3. Finally, the paper is concluded in Section 4.

2. Methodology

In this study, our target was to classify machine faults under variable speed conditions (i.e., RPM) in a transfer learning manner. There are three major steps in the proposed methodology: the source task, transfer, and target task. In the source task, we first apply a new preprocessing technique for the collected acoustic emission (AE) data to transform the 1D signal into a 2D image, which is referred to as acoustic spectral imaging (ASI). This allows us to visualize the bearing health condition, and the 2D images are fed to the convolutional neural network (CNN) for model parameter optimization. The transfer block mainly passes the knowledge gathered from the source task network to the target network to complete the transfer learning (TL). In the target task, we test the model for classifying faults for variable RPMs. Figure 1 provides a clear illustration of the entire process.
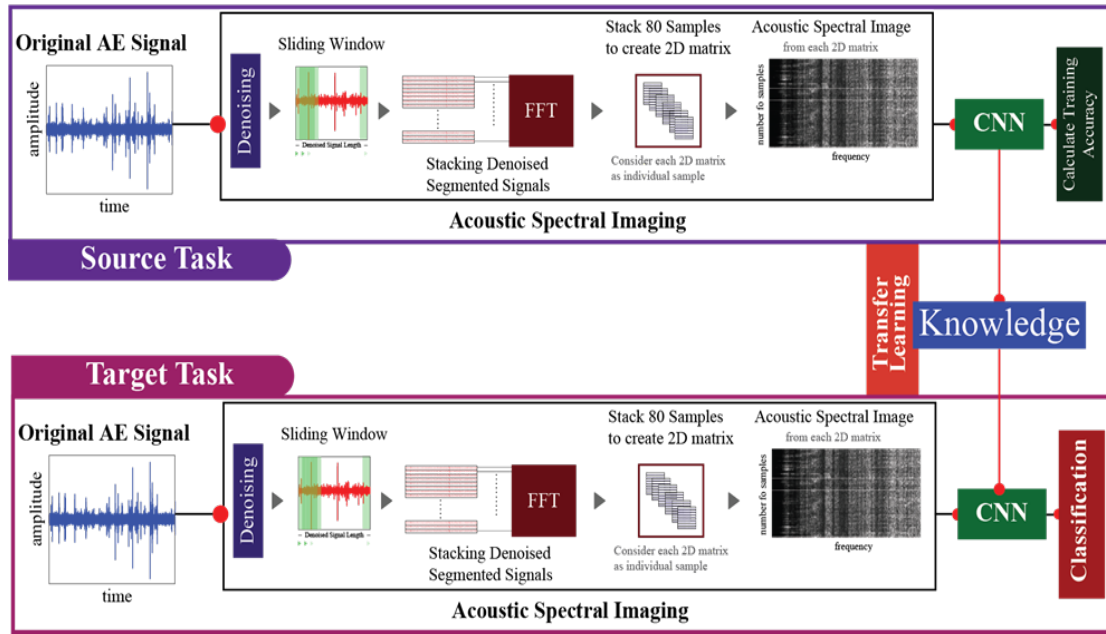
Figure 1: Overall approach for the proposed methodology.

2.1. Experimental testbed and data acquisition

An experiment was conducted on a self-designed test rig to collect acoustic emissions (AE) signals, as shown in Figure 2. As the main purpose of this study is to diagnose faults for variable RPMs, the test rig was driven at three different motor speeds of 250, 300, and 350 RPMs. This setup has two shafts, namely a drive end shaft (DES) and a non-drive end shaft (NDES). A three-phase induction motor is positioned in the DES at three different speeds (i.e., 250, 300, and 350 revolutions per minutes (rpm)) and the bearing house is connected to the motor shaft through a gearbox with a reduction ratio of 1.52:1. At the NDES, a WSα AE sensor is positioned over the bearing house in the shaft. To quantify the functioning speed, a displacement transducer is installed on the NDES. Figure 2(a) shows the test rig and the PCI-2 based data acquisition system is shown in Figure 2(b). Bearings with three defect conditions of an inner raceway crack (IRC), outer raceway crack (ORC), and roller raceway crack (RRC) as well as one normal condition (NC) bearing were used to simulate faults for each RPM. The test bearings with a fault size of 6 mm are shown in Figure 3. Bearing AE signals were collected at a sampling rate of 25,000 Hz. Additional studies involving the experiment test rig and data acquisition system can be found elsewhere[34, 35].

2.2. Acoustic Spectral Imaging (ASI) for Bearing Health State Visualization

As explained in Section 1, bearing characteristic frequencies are not observable in raw AE signals. Therefore, it is essential to define an appropriate visualization tool that reveals a unique pattern regarding the health state of a bearing. Consequently, we developed a 2D ASI tool that generates an identical health pattern even with various RPMs for each fault type (e.g., NC, IRC, ORC, and RRC). It is important to provide the full advantages of the 2D structure to the deep neural network with these identical patterns. To carry out the ASI, several steps must be performed. The steps of the proposed ASI are shown in Figure 4 and the detailed process is given below.
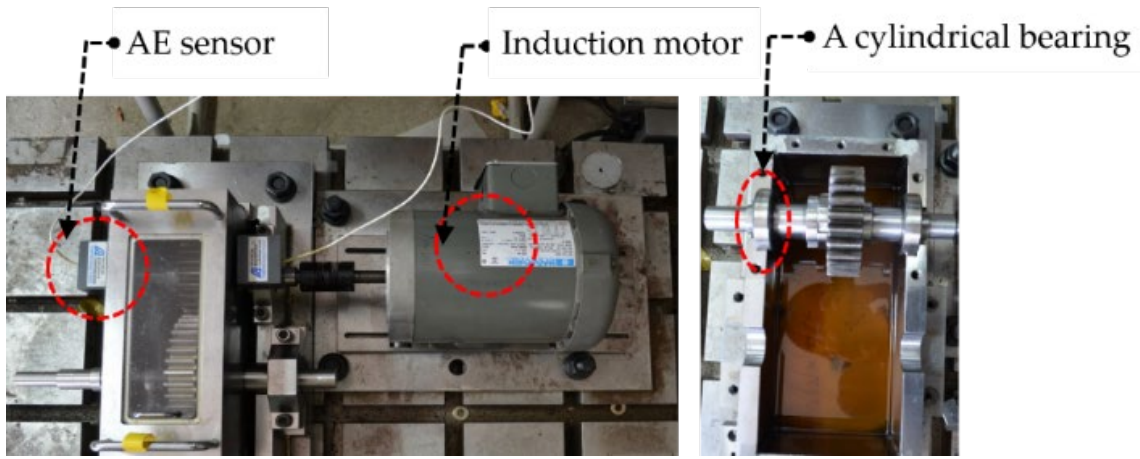
Figure 2: (a) Experimental testbed and (b) data acquisition system.

Figure 3: Examples of ORC, IRC, and RRC bearing defects.
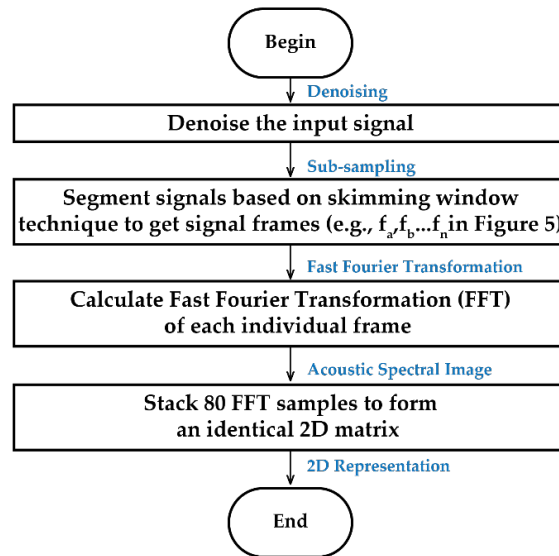
Figure 4: Flowchart of the acoustic spectral imaging (ASI) for visualization of the bearing health condition.

The performance of the ASI analysis can be improved if the variations between the flanks and peaks of the spectral energy, which mainly originate from noise from various sources, are minimized. Therefore, we applied a denoising technique known as pre-whitening before ASI[36]. In this paper, the pre-whitening technique is used to reduce the spectral energy variations in the incoming AE fault signal, as can be seen in Figure 4. To obtain the pre-whitened signal, an autoregressive (AR) model, $x(n)$, is utilized, which is defined as follows.

$$x(n) = \sum_{i=1}^{k} a_i y(i+n) + e(n) \tag{1}$$

Here, $y(n)$ is the incoming bearing signal, a_i are the AR coefficients, k denotes the order of the AR model, and $e(n)$ is the residual signal representing a spectrum close to the white noise spectrum.

Processing this lengthy 1D data necessitates an enormous computational time. To handle these issues, an adjustable skimming window mechanism is proposed[33]. This technique aims to achieve (a) efficient training of the network by cutting down repetitive AE signals into small segments, which will eventually yield a good amount of source data for training, (b) handling the issue of fitting the lengthy amount of data to the network as input through segmentation, and (c) stacking segmented AE signals together. This can be useful to further process and generate some identical patterns via imagining, which can be fed to the proposed neural network for classification. If the total length of the AE signal is A_{Lt}, then the total number of the samples A_{Nt} is as follows.

$$A_{Nt} = \left(\frac{A_{Lt} - A_{Lf}}{A_{Ls}} \right) + 1 \tag{2}$$

Here, A_{Lf} denotes the length of a single frame, f ($f = f_a, f_{b,\ldots\ldots\ldots}, f_n$) and the step size is A_{Ls}. The complete process of the adjustable skimming window technique is illustrated in Figure 5.
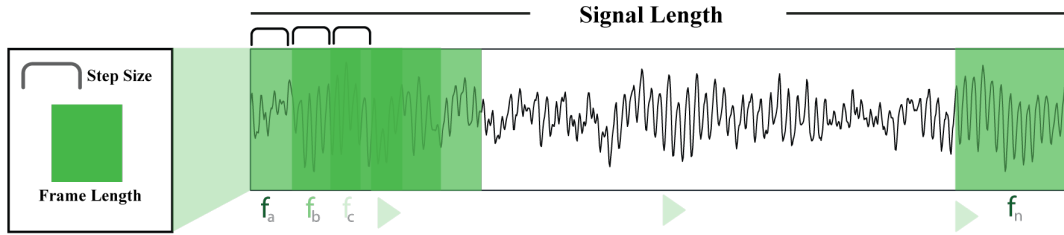
Figure 5: Adjustable sliding window technique.

We applied the Fast Fourier Transformation (FFT) to each segmented signal. If S_N is the number of total samples, then FFT will perform $s_N \times \log(S_N)$ operations. The reasons behind using this FFT are gathering better analysis of the denoised signals based on the frequency domain and creating identical images from stacked signals. For each health type, conversion of denoised signals into frequency domain results in identical visual patterns. In our experiment, it was demonstrated that frequency resolution could provide identical patterns. FFT of each sample is based on the Nyquist theorem and half of the data points in the frequency spectrum are considered.

Then, the stack of the preprocessed signals forms identical patterns for each health type. The images are larger when stacking many segmented signals. To handle this issue, in this study, the height of the stacked signals for generating identical images was fixed based on experiments. If the total number of segmented signals is Z and each segment has a length of W, then the size of the image is $Z \times W$ ($Height \times Width$). This height is very large as well as challenging to feed to the proposed network. Therefore, to generate small sized images, a number of samples z is considered from the Z segmented samples (where $z \in Z, z < Z$ and $Z > 80$) and then $z \times W$ sized

images are bunched together to be fed to the network. In this study, $z = 80$ can generate better resolution for ASI from the denoised frequency resolution.

2.3. Transfer Learning with CNN for fault classification under variable RPMs

The proposed classification approach with transfer learning was developed on convolutional neural networks. A convolutional neural network (CNN) may lead to a better performance itself, but to achieve substantial performance, a significant amount of training parameters are required to optimize. The performance of the CNN can generally be improved by increasing the number of layers. More layers will add more trainable parameters. However, training this vast number of parameters requires a substantial number of valid training samples. Compared to natural language processing or image classification, the amount of data is not sufficient in the field of bearing fault classification. It is irrational to gather physical data from each health condition and especially severity since the severity level is continuous and there are an infinite number of possible health profiles. In this study, for a different speed, the health profiles vary as well. With the preprocessing step, the health profile can get an invariant overview, yet the minor details of the patterns are also significant while measuring the network performance. This issue is well balanced by the CNN with TL. From one working condition, the gathered knowledge for the source network is passed to the target network and by using that knowledge with a small amount of data, the deeper architecture of the network can learn well. Moreover, the minor details of the health patterns also remain under consideration because the learnings are transferred, and the fine-tuned and trained parameters help the target task parameters to be fine-tuned in a balanced way. The usage of TL with the CNN brings robustness to the network performance for this speed invariance situation. In this section, the essential formulation of our proposed CNN architecture and transfer learning is discussed to portray a clear overview.

CNN has a feedforward network structure composed of several convolutional, subsampling, and fully connected layers. In practice, without the input and output layers, the other layers are considered as a hidden layer, which makes the best usage of the indigenous connections and weight distributions to achieve consistency for shifting, scaling, and distortion of the inputs[37]. These hidden layers make the feature selection process automated through backpropagation. An intuitive mathematical overview of a three-layer CNN (i.e., input, hidden, and output layers) is considered, where S_S and N are the input and output vectors, respectively. The hidden vector is symbolized as H_{vec}. The feedforward method is shown below.

$$H_{vec} = \sigma_{ac}(\omega_1 S_S + \beta_1) \tag{3}$$

$$N = \sigma_{ac}(\omega_2 H_{vec} + \beta_2) \tag{4}$$

$$\sigma_{ac}(\text{x}) = \frac{1}{1+e^{-x}} \tag{5}$$

Here, ω_1 is the weight matrix between the input and hidden layer, and ω_2 the weight matrix between the hidden and output layer. The bias vectors of the hidden and output layers are denoted as β_1 and β_2, respectively. $\sigma_{ac}(.)$ is the sigmoid activation function. The loss function is shown below,

$$F_{LS} = \frac{1}{n}\sum_{i=1}^{n} \| \mathbf{m}_i . \ln N_i + (1+m_i).\ln(1-N_i) \|_1 , \tag{6}$$

where m_i represents the target vector and n denotes the number of training samples. The target of this network is to minimize the loss function F_{LS} through backpropagation and gradient descent (GD)[33]. In this study, the proposed network has a depth of nine layers (one is the output layer). As in practice, the pooling layer does the subsampling of data from the convolution layer to reduce the spatial size of the representation where the dropout layer assists the network to avoid over-fitting[38]. Stochastic gradient descent (SGD) is applied for tuning the network. The classifier used for the network setup is SoftMax. Figure 6 illustrates the full network model. After completion of the training with the source data, the final output ω_S can be obtained as follows.

$$\omega_S = f_s \left(S_S, \theta_S \right) \tag{7}$$

Here, θ_S denotes the cost function for the source sample and f_s is the mapping function.
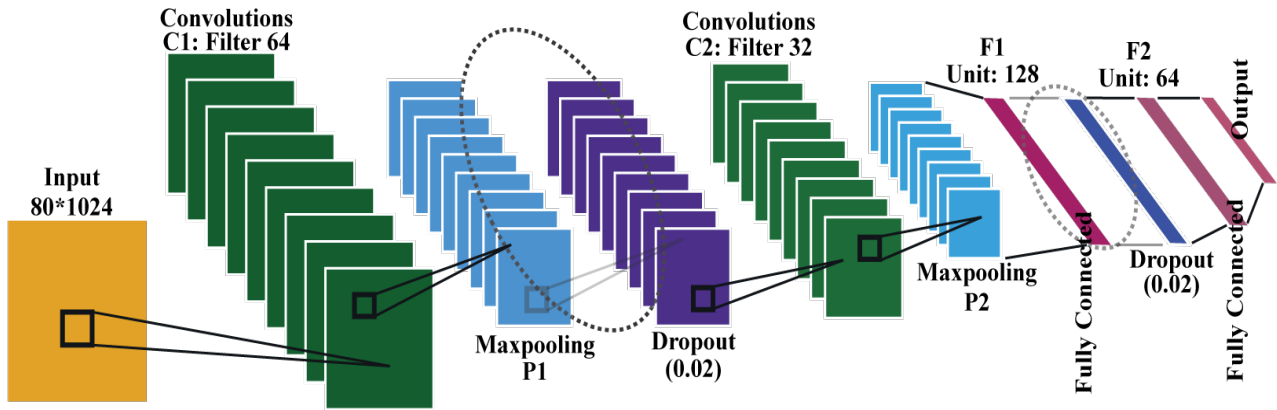
Figure 6: The detailed architecture of the proposed 2D CNN.

Now, if the proposed network is trained with target data, similar to equation (7) for the target data, the final output ω_T is obtained in a similar manner, where S_T is the input, θ_T denotes the cost function for source sample, and f_T is the mapping function.

$$\omega_T = f_T \left(S_T, \theta_T \right) \tag{8}$$

In transfer learning, TL discovers the related properties in the source task and obtains the mapping function f_S in the source domain. Then it transfers f_S to the target task and learns the task f_T. Therefore, the goal of TL is to expand the learning performance of a target domain by using the knowledge of the source domain[37]. Figure 7 demonstrates the main concept of TL.

In the TL approach, the first well-trained d layers of the source network are transferred to the target network which contains e number of layers ($e > d$). At the initial condition, the last ($e-d$) layers of the target network remain untrained. They begin training with the target data by utilizing the knowledge acquired through the transfer of the d layers, which finally gives the fine-tuned output ω_T of the target task. The dimensions of the proposed CNN architecture with the details of transferrable layers are shown in Table 1.
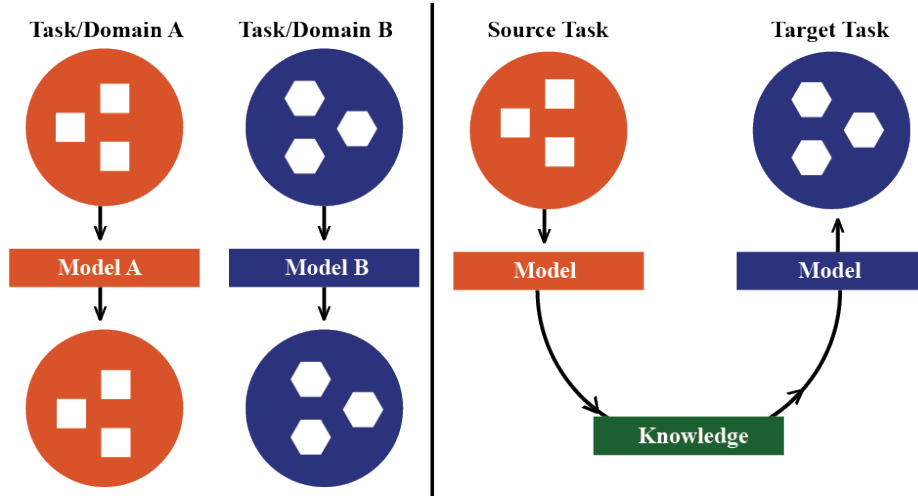
Figure 7: On the left-hand side, the conventional learning process is described. On the right-hand side, the concept of transfer learning is illustrated.

Table 1. The dimensions of the proposed Convolutional Neural Network with the transfer specification for the target network.

Layers	Parameters	Remarks	Height	Width	Depth	Parameters Trainable	Transfer
Input		Preprocessed Signals	80	512	1		
Conv. 1	Kernel Size	Filter	3	3		Yes	Yes
	Padding	Same					
	Depth	Filter number			32		
	Output		80	512	32		
Pool 1	Kernel Size	Filter	3	3		No	Yes
	Padding	Same					
	Output		27	171	32		
Dropout	Output		27	171	32	No	Yes
Conv. 2	Kernel Size	Filter	3	3		Yes	Yes
	Padding	Same					
	Depth	Filter number			64		
	Output		27	171	64		
Pool 2	Kernel Size	Filter	3	3		No	Yes
	Padding	Same					
	Output		9	57	64		
Dropout	Output		9	57	64	No	Yes
FC	Nodes	Flatten into 1D	128			Yes	No
SoftMax	Nodes	Flatten into 1D	4			Classify	No

Therefore, once the 2D ASI of the AE signal is obtained, the proposed 2D CNN architecture is used for multi-fault classification by utilizing transfer learning. As mentioned at the beginning, the deeper layers of the neural network will add more trainable parameters, which requires a lot of training data. As a result, TL helps to resolve this issue. In addition, the slight variance in the obtained health patterns are also under consideration as the mapping function of source task f_s is passed to the target task to fine-tune the final weights of the target task to generate final output ω_T .

3. Results and Discussion

3.1. Dataset description

For investigation of the appropriateness of the proposed fault diagnosis scheme including ASI-based RPM invariant bearing health state visualization and transfer learning RPM invariant bearing fault classification, extensive simulation and experimental analyses are presented in this section. The benchmark AE dataset of bearing faults was used to conduct the experiments. We used three different RPMs (250, 300, and 350) and recorded 110 signals for each fault type (e.g., NC, IRC, ORC, and RRC) at each RPM. The details of the dataset are given in Table 2.

Table 2. Details of the considered working conditions with the same health types.

	Health Type	Shaft Speed (rpm)	Number of Singles, with Sampling Frequency (250K Hz) and Signal Length (1 sec)	Crack Size
				Length (mm)
Dataset 1	Normal Condition (NC)	250		6
	Inner Race Fault Condition (IRC)	250		6
	Outer Race Fault Condition (ORC)	250		6
	Roller Raceway Fault Condition (RRC)	250		6
Dataset 2	Normal Condition (NC)	300		6
	Inner Race Fault Condition (IRC)	300		6
	Outer Race Fault Condition (ORC)	300	110	6
	Roller Raceway Fault Condition (RRC)	300		6
Dataset 3	Normal Condition (NC)	350		6
	Inner Race Fault Condition (IRC)	350		6
	Outer Race Fault Condition (ORC)	350		6
	Roller Raceway Fault Condition (RRC)	350		6

3.2. Performance Analysis of Acoustic Spectral Imaging (ASI)

As explained in Section 1, the 1D signal reveals no distinguishable patterns regarding faults and almost no information about RPM variance, as can be seen in Figure 8. Therefore, we developed 2D-based ASI to represent the bearing health state. To visualize the effectiveness of ASI, this paper utilizes three datasets with four fault types (NC, IRC, ORC, and RRC) at various operating conditions (see Table 2). Figure 9 presents the results of the 2D-based ASI for bearing health state representation. According to the results in Figure 9, it is apparent that the frequency band as a function of time for different health conditions yields different patterns. In the considered dataset, though the rpm varies, the pattern remains identical and distinguishable for different health types. In short, the same type of health conditions generates the same kind of patterns where they remain identical to the others. This is because the 1D AE signal is proposed in a way so that all time information is stacked together for converting into a 2D image to utilize the distribution of energies in various frequency bands.
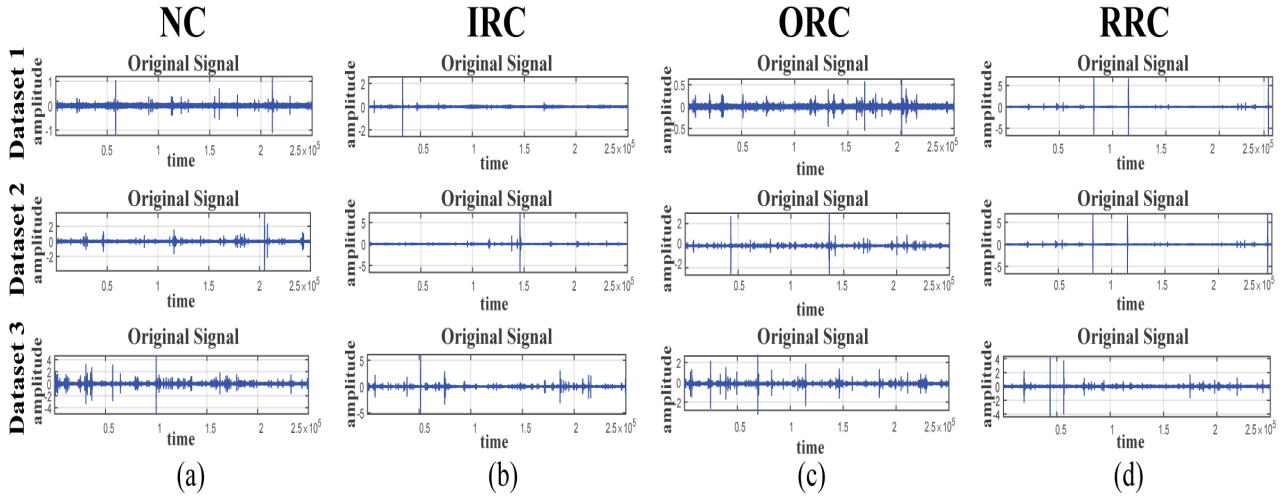
Figure 8: Different raw signals for different health conditions: (a) NC, (b) IRC, (c) ORC, and (d) RRC.
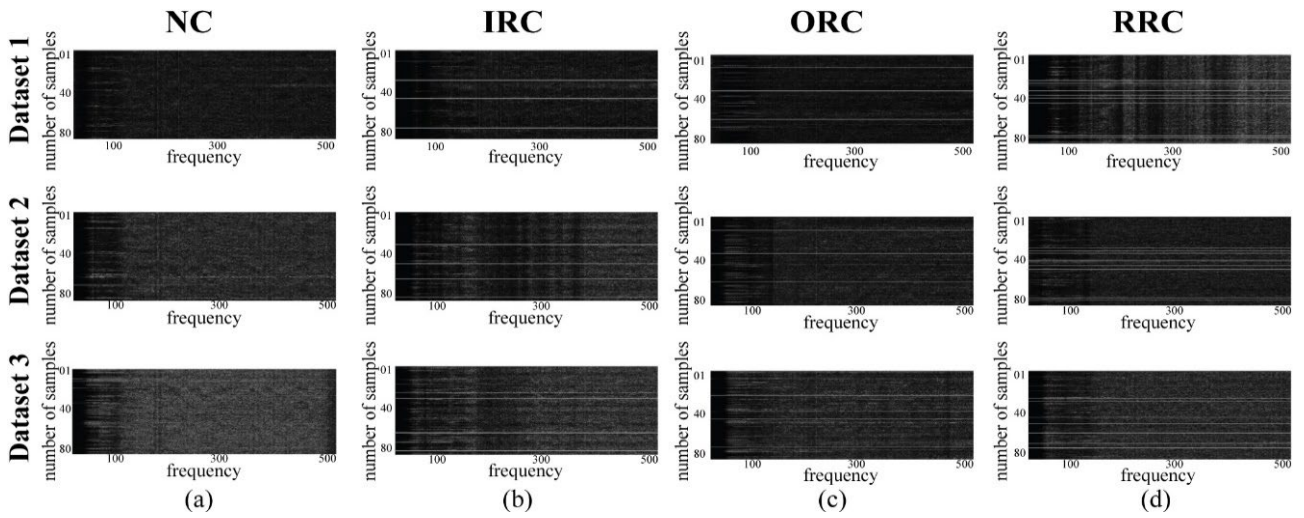
Figure 9: Different ASI for different health conditions: (a) NC, (b) IRC, (c) ORC, and (d) RRC.

3.3. Diagnostic performance of the proposed method

As our proposed ASI is highly effective to visualize the performance of bearing health representation, to further take full advantage of the 2D-CNN architecture, we used ASI as an input to the CNN for diagnosing bearing faults under variable speeds.

To authenticate the performance of the proposed TL-based method, it is essential to divide the dataset into appropriate training and testing. In the first scenario, dataset 1 is used to train the network and store the knowledge, whereas datasets 2 and 3 utilize the stored knowledge to perform the classification test. From datasets 2 and 3, 20% of the data is used for adjusting the network to use the prior knowledge. In the second scenario, dataset 2 is used for gathering the knowledge and datasets 3 and 4 are used for TL-based testing. Similarly, in scenario 3, dataset 3 is used for knowledge gathering, whereas datasets 1 and 2 are used for classification. In each scenario, one dataset is known to the network and the other datasets utilize the learning knowledges to make the learning faster and efficient by maintaining the TL principle to archive the accuracy. Table 3 provides the classification results. In the results, it is seen that the proposed TL-based bearing fault

diagnosis under variable RPMs is outperformed. The average classification accuracies of the different health types for target conditions are 99.73%, 88.14%,97.04% and 94.78% for NC, IRC, ORC, and RRC, respectively. The overall classification accuracy is 94.67%. For each scenario, the test dataset is 5 times higher than the training set which means that TL can work effectively even when the operation conditions change. To fine-tune the network and to obtain classification accuracy, 300 fine-tuned epochs are used.

Table 3. Diagnostic performance of the proposed model under different scenarios.

Scenario	Target Dataset	Source Dataset	Classification Accuracy (%)				Average Classification Accuracy (%)	Overall Classification Accuracy (%)
			NC	IRC	ORC	RRC		
1	Dataset 1	Dataset 2	98.30	84.23	95.77	92.87	92.79	93.995
		Dataset 3	99.81	89.37	96.28	95.34	95.20	
2	Dataset 2	Dataset 3	99.38	88.85	96.84	95.53	95.14	95.615
		Dataset 1	97.68	90.27	98.87	97.58	96.09	
3	Dataset 3	Dataset 1	98.24	87.99	98.64	97.23	95.53	94.4
		Dataset 2	98.97	88.12	95.86	90.13	93.27	
Average Accuracy			98.73	88.14	97.04	94.78	94.67	

To further investigate the performance, we analyzed the training and validation performance of our proposed TL method. For scenario 1, dataset 1 is used for training and saving knowledge, whereas datasets 2 and 3 are utilized for testing. First, the CNN with the proposed architecture is trained with dataset 1. After achieving a training accuracy of 96% (see Figure 10(a)), the assembled knowledge is transferred to the target conditions. For this source task, 80% of the data is used for training and other 20% is used for validation.
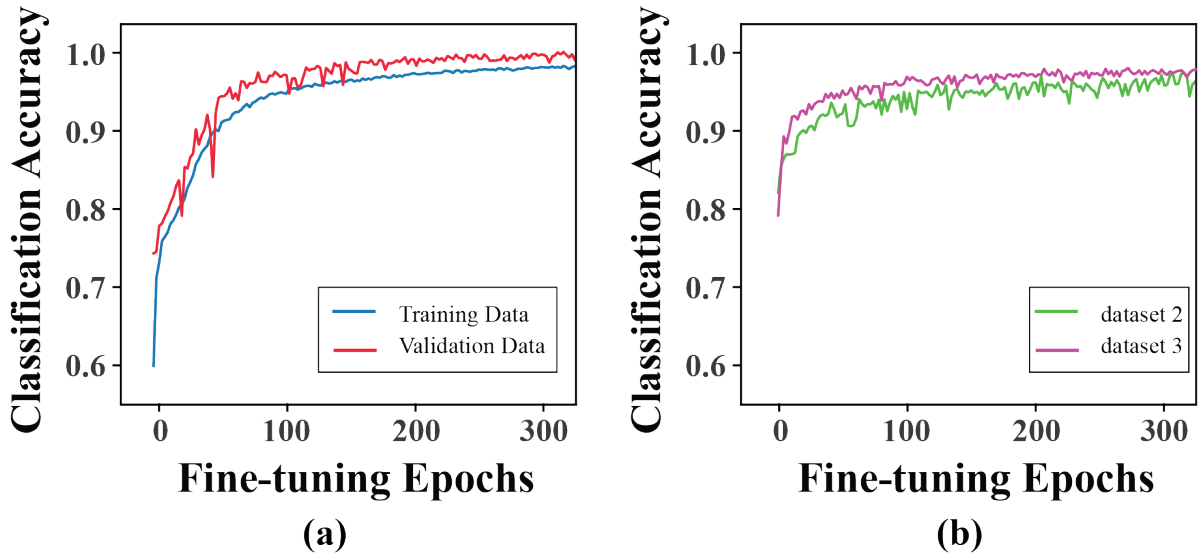
Figure 10: (a) The training and validation accuracy curve for the source task (dataset 1) and (b) the testing accuracy with transfer learning for the target task (datasets 2 and 3).

In Figure 10(b), datasets 2 and 3 achieve accuracies of 92.79% and 95.20%, respectively. We also provide the results of the confusion matrix. The confusion matrix is a robust technique which visualizes the classification

performance in terms of actual vs. predicated[38]. Figure 11 provides the confusion metrics results for scenario 1 where datasets 2 and 3 are targets, and dataset 1 is training.
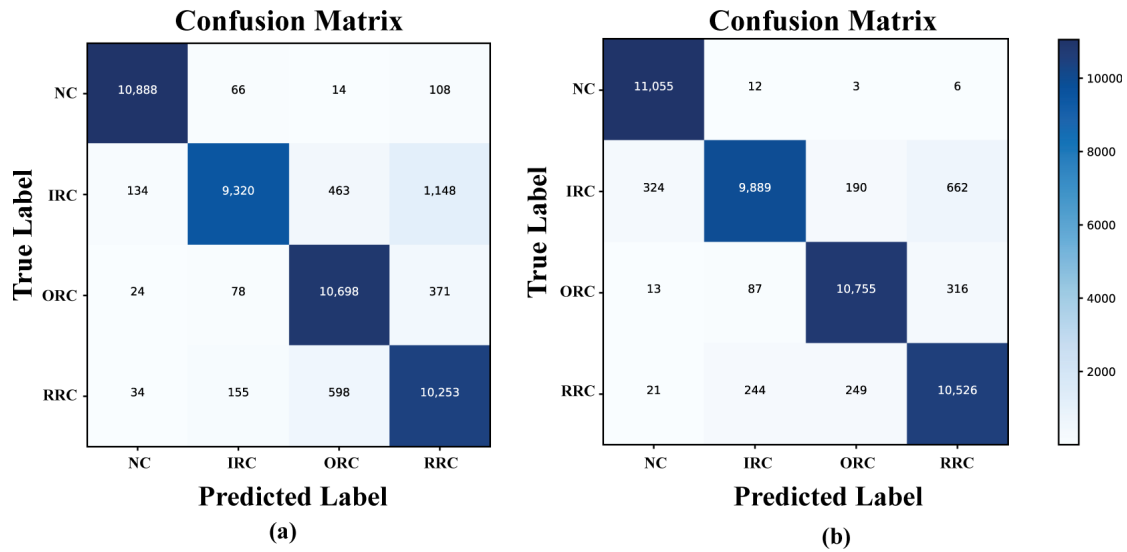
Figure 11: The confusion matrices for showing classification results for different health types of (a) dataset 2 and (b) dataset 3.

To establish the robustness of this approach, several comparisons are considered. First, we compare the performances with and without TL (conventional CNN). In this case, the network is trained and tested on dataset 2, where 20% of the data is used for training and 80% for testing. Here, the ratio of training and testing is kept like TL-based scenarios to compare the performances. In Figure 12(a), we can observe that the conventional approach using 20% of the data for training, an overall classification accuracy of around 85% is achieved whereas our proposed approach can provide an overall accuracy of 92.79%. However, for further analysis, from the learning epochs, one obvious thing is that the TL-based approach can save time to achieve the desired accuracy (see Figure 12(b)). This clearly proves that the TL-based approach can yield the desired accuracy faster.
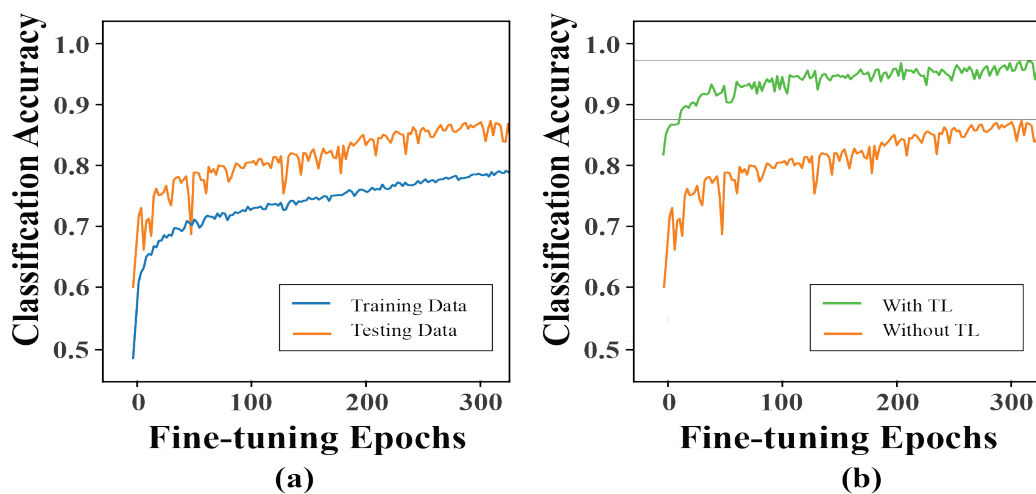
Figure 12: (a) The classification accuracy of dataset 2 obtained conventionally (without TL, where train: test = 20:80) and (b) classification accuracy comparison between the two approaches (with TL and without TL).

Second, we compared our proposed method with a state-of-the-art TL-based method with a raw 1D signal[33]. Table 4 compares the results of the proposed scheme and the raw signal-based TL approach[33]. It is clearly seen that our ASI with the TL-based method outperforms its counterpart. Our proposed approach can yield at least an overall improvement of 23% of the final performance.

Table 4. Comparison of the classification accuracy between the existing TL approach and the proposed ASI-based TL approach.

Scenario	Method	Classification Accuracy (%)				Average Classification Accuracy (%)	Improvement (%)
		NC	IRC	ORC	RRC		
1	Raw+TL[33]	74.21	64.2	71.12	73.58	70.78	**23.21**
	Proposed	99.06	86.8	96.03	94.11	93.99	
2	Raw+TL[33]	72.56	63.62	70.59	74.22	70.23	**25.39**
	Proposed	98.53	89.56	97.86	96.56	95.62	
3	Raw+TL[33]	72.44	66.31	70.23	73.39	70.59	**23.81**
	Proposed	98.61	88.06	97.25	93.68	94.4	

4. Conclusions

This study presents two-dimensional acoustic frequency spectral imaging with a transfer learning-based fault diagnosis method that adds a new dimension to bearing fault diagnosis, which is invariant to both random and deliberate differences of the shaft speed. In traditional approaches, the diagnosis of the bearing is mainly based on detecting defect frequencies. These techniques have certain challenges, for example, a non-stationary shaft speed creates an impact on defect frequencies, and variations of the shaft speeds bring significant and tiny variations on defect frequencies. In addition to this, the conventional feed-forward neural network mechanisms lack autonomous feature extraction for improving classification performance as in the CNN and TL. This study validated our proposed method by using the health images of four different health conditions for three different rotational speeds. The TL-based network yields an average accuracy of 94.67%, which establishes this proposed method as invariant to variations of shaft speed. A comparison with a recent TL trend clearly shows that the proposed method provides better accuracy.

Acknowledgment

References

[1] S.A. Khan, J.M. Kim, Automated Bearing Fault Diagnosis Using 2D Analysis of Vibration Acceleration Signals under Variable Speed Conditions, Shock and Vibration, 2016 (2016).
[2] R. Saidur, A review on electrical motors energy use and energy savings, Renewable and Sustainable Energy Reviews, 14 (2010) 877-898.
[3] I. El-Thalji, E. Jantunen, Dynamic modelling of wear evolution in rolling bearings, Tribology International, 84 (2015) 90-99.

[4] O.V. Thorsen, M. Dalva, Failure identification and analysis for high-voltage induction motors in the petrochemical industry, IEEE Transactions on Industry Applications, 35 (1999) 810-818.

[5] R. Zhang, Z. Peng, L. Wu, B. Yao, Y. Guan, Fault Diagnosis from Raw Sensor Data Using Deep Neural Networks Considering Temporal Coherence, Sensors, 17 (2017) 549.

[6] X. Jiang, L. Wu, M. Ge, A novel faults diagnosis method for rolling element bearings based on ewt and ambiguity correlation classifiers, Entropy, 19 (2017).

[7] M. Sohaib, C.-H. Kim, J.-M. Kim, A Hybrid Feature Model and Deep-Learning-Based Bearing Fault Diagnosis, Sensors, 17 (2017) 2876.

[8] S. Li, G. Liu, X. Tang, J. Lu, J. Hu, An Ensemble Deep Convolutional Neural Network Model with Improved D-S Evidence Fusion for Bearing Fault Diagnosis, Sensors, 17 (2017) 1729.

[9] V. Tra, J. Kim, S.A. Khan, J.-M. Kim, Incipient fault diagnosis in bearings under variable speed conditions using multiresolution analysis and a weighted committee machine, The Journal of the Acoustical Society of America, 142 (2017) EL35-EL41.

[10] S. Zhao, L. Liang, G. Xu, J. Wang, W. Zhang, Quantitative diagnosis of a spall-like fault of a rolling element bearing by empirical mode decomposition and the approximate entropy method, Mechanical Systems and Signal Processing, 40 (2013) 154-177.

[11] Y. Song, S. Zeng, J. Ma, J. Guo, A fault diagnosis method for roller bearing based on empirical wavelet transform decomposition with adaptive empirical mode segmentation, Measurement, 117 (2018) 266-276.

[12] S. Yin, S.X. Ding, D. Zhou, Diagnosis and prognosis for complicated industrial systems - Part i, IEEE Transactions on Industrial Electronics, 63 (2016) 2501-2505.

[13] S. Yin, S.X. Ding, D. Zhou, Diagnosis and Prognosis for Complicated Industrial Systems—Part II, IEEE Transactions on Industrial Electronics, 63 (2016) 3201-3204.

[14] W. Huang, H. Sun, W. Wang, Resonance-based sparse signal decomposition and its application in mechanical fault diagnosis: A review, Sensors (Switzerland), 17 (2017).

[15] X. Qin, Q. Li, X. Dong, S. Lv, The Fault Diagnosis of Rolling Bearing Based on Ensemble Empirical Mode Decomposition and Random Forest, 2017 (2017).

[16] T. Han, D. Jiang, Y. Sun, N. Wang, Y. Yang, Intelligent fault diagnosis method for rotating machinery via dictionary learning and sparse representation-based classification, Measurement, 118 (2018) 181-193.

[17] L. Frosini, E. Bassi, Stator current and motor efficiency as indicators for different types of bearing faults in induction motors, IEEE Transactions on Industrial Electronics, 57 (2010) 244-251.

[18] E.C.C. Lau, H.W. Ngan, Detection of motor bearing outer raceway defect by wavelet packet transformed motor current signature analysis, IEEE Transactions on Instrumentation and Measurement, 59 (2010) 2683-2690.

[19] A. Soualhi, G. Clerc, H. Razik, Detection and diagnosis of faults in induction motor using an improved artificial ant clustering technique, IEEE Transactions on Industrial Electronics, 60 (2013) 4053-4062.

[20] B. Eftekharnejad, M.R. Carrasco, B. Charnley, D. Mba, The application of spectral kurtosis on Acoustic Emission and vibrations from a defective bearing, Mechanical Systems and Signal Processing, 25 (2011) 266-284.

[21] A. Widodo, E.Y. Kim, J.D. Son, B.S. Yang, A.C.C. Tan, D.S. Gu, B.K. Choi, J. Mathew, Fault diagnosis of low speed bearing based on relevance vector machine and support vector machine, Expert Systems with Applications, 36 (2009) 7252-7261.

[22] D.H. Pandya, S.H. Upadhyay, S.P. Harsha, Fault diagnosis of rolling element bearing with intrinsic mode function of acoustic emission data using APF-KNN, Expert Systems with Applications, 40 (2013) 4137-4145.

[23] S.A. Niknam, V. Songmene, Y.H.J. Au, The use of acoustic emission information to distinguish between dry and lubricated rolling element bearings in low-speed rotating machines, International Journal of Advanced Manufacturing Technology, 69 (2013) 2679-2689.

[24] W. Caesarendra, P.B. Kosasih, A.K. Tieu, C.A.S. Moodie, B.K. Choi, Condition monitoring of naturally damaged slow speed slewing bearing based on ensemble empirical mode decomposition, Journal of Mechanical Science and Technology, 27 (2013) 2253-2262.

[25] P. Nguyen, M. Kang, J.M. Kim, B.H. Ahn, J.M. Ha, B.K. Choi, Robust condition monitoring of rolling element bearings using de-noising and envelope analysis with signal decomposition techniques, Expert Systems with Applications, 42 (2015) 9024-9032.

[26] R.B. Randall, J. Antoni, Rolling element bearing diagnostics-A tutorial, Mechanical Systems and Signal Processing, 25 (2011) 485-520.

[27] M. Kang, J. Kim, J.-m. Kim, High-Performance and Energy-Efficient Fault Diagnosis Using Effective Envelope Analysis Processing Unit, IEEE Transactions on Power Electronics, 30 (2015) 2763-2776.

[28] M. Cerrada, R. Sánchez, D. Cabrera, G. Zurita, C. Li, Multi-Stage Feature Selection by Using Genetic Algorithms for Fault Diagnosis in Gearboxes Based on Vibration Signal, Sensors, 15 (2015) 23903-23926.

[29] M. Kang, J. Kim, J.M. Kim, A.C.C. Tan, E.Y. Kim, B.K. Choi, Reliable fault diagnosis for low-speed bearings using individually trained support vector machines with kernel discriminative feature analysis, IEEE Transactions on Power Electronics, 30 (2015) 2786-2797.

[30] H. Zhou, T. Shi, G. Liao, J. Xuan, J. Duan, L. Su, Z. He, W. Lai, Weighted kernel entropy component analysis for fault diagnosis of rolling bearings, Sensors (Switzerland), 17 (2017).

[31] S. Malek, F. Melgani, Y. Bazi, One-dimensional convolutional neural networks for spectroscopic signal regression, Journal of Chemometrics, (2017) 1-17.

[32] A. Prosvirin, J. Kim, J.M. Kim, Bearing fault diagnosis based on convolutional neural networks with kurtogram representation of acoustic emission signals, Lecture Notes in Electrical Engineering, 474 (2018) 21-26.

[33] R. Zhang, H. Tao, L. Wu, Y. Guan, Transfer Learning with Neural Networks for Bearing Fault Diagnosis in Changing Working Conditions, IEEE Access, 5 (2017) 14347-14357.

[34] M.M.M. Islam, J. Myon, Time–frequency envelope analysis-based sub-band selection and probabilistic support vector machines for multi-fault diagnosis of low-speed bearings, Journal of Ambient Intelligence and Humanized Computing, 0 (2017) 0.

[35] V. Tra, J. Kim, S.A. Khan, J.-M. Kim, Bearing Fault Diagnosis under Variable Speed Using Convolutional Neural Networks and the Stochastic Diagonal Levenberg-Marquardt Algorithm, Sensors, 17 (2017) 2834.

[36] P. Borghesani, P. Pennacchi, R.B. Randall, N. Sawalhi, R. Ricci, Application of cepstrum pre-whitening for the diagnosis of bearing faults under variable speed conditions, Mechanical Systems and Signal Processing, 36 (2013) 370-384.

[37] Y. LeCun, L. Bottou, Y. Bengio, P. Haffner, Gradient-based learning applied to document recognition, Proceedings of the IEEE, 86 (1998) 2278-2323.

[38] M.M.M. Islam, J.-M. Kim, Motor Bearing Fault Diagnosis Using Deep Convolutional Neural Networks with 2D Analysis of Vibration Sign, Advances in Artificial Intelligence, 2671 (2003) 520-526.